

# Tunneling maps, non-monotonic resistivity, and non Drude optics in $\text{EuB}_6$

Tanmoy Mondal and Pinaki Majumdar

Harish-Chandra Research Institute (A CI of Homi Bhabha National Institute), Chhatnag Road, Jhusi, Allahabad 211019

(Dated: August 8, 2024)

For several decades the low carrier density local moment magnet  $\text{EuB}_6$  has been considered a candidate material for ferromagnetic polarons. There is however no consistent explanation for the host of intriguing observations that have accrued over the years, including a prominently non-monotonic resistivity near  $T_c$ , and observation of spatial textures, with a characteristic spatial and energy scale, via scanning tunneling spectroscopy. We resolve all these features using a Heisenberg-Kondo lattice model for  $\text{EuB}_6$ , solved using exact diagonalisation based Langevin dynamics. Over a temperature window  $\sim 0.7T_c - 1.5T_c$  we observe electronic and magnetic textures with the correct spatial and energy scale, and confirm an associated non-monotonic resistivity. We predict a distinctly ‘non Drude’ optical conductivity in the polaronic phase, and propose a field-temperature phase diagram testable through spin resolved tunneling spectroscopy. We argue that the anomalous properties of  $\text{EuB}_6$ , and magnetic polaron materials in general, occur due to a non monotonic change in spatial character of ‘near Fermi level’ eigenstates with temperature, and the appearance of a weak pseudogap near  $T_c$ .

Ferromagnetic polarons (FP) were proposed first in the context of Eu based magnetic semiconductors in the 1960s [1, 2]. Most of these materials display metallic resistivity,  $d\rho/dT > 0$ , at low temperature, a strong peak around the ferromagnetic  $T_c$ , and a wide window with  $d\rho/dT < 0$  thereafter [2–8]. It was suggested [6–10] that electrons in these low carrier density systems, while delocalised in the ferromagnetic state, get ‘self trapped’ in the paramagnetic state - creating a small polarised region and gaining energy by localising there. Over the decades the transport in a large number of local moment ferromagnets has been attributed to FP [3–8].

The intuitive physical picture has proved hard to convert to a concrete theory that addresses the accumulated data consistently. The best documented material is  $\text{EuB}_6$  [11–28], a local moment ferromagnet with  $S = 7/2$  moments arising from Eu, low carrier density,  $n \sim 10^{-2}$  carriers per formula unit, and a  $T_c \sim 15\text{K}$ . Raman scattering [14] and muon spin relaxation [15] had suggested an inhomogeneous electronic-magnetic state near  $T_c$ . The most unconventional features however are: (i) The d.c resistivity, which shows a maximum near  $T_c$ , and then a shallow minimum at  $T \sim 2T_c$ , with the maximum-minimum feature suppressed by a field of  $\sim 0.3$  Tesla [16, 17]. (ii) Scanning tunneling spectroscopy (STS) [18], which reveals a spatial inhomogeneity in local conductance near  $T_c$  - with the textures having a linear dimension  $\sim 8$  lattice spacings and a showing tunneling peak at  $\sim 25\text{mV}$  below Fermi level. These key experiments remain unexplained.

Several theoretical attempts have been made to model the magnetic polaron problem [29–32] and also specifically address the properties of  $\text{EuB}_6$  [33–37]. These include study of a polaron hopping model [33] to address the  $T \gg T_c$  resistivity, a small,  $8 \times 8$ , lattice Monte Carlo to explain the specific heat [36, 37] in terms of ‘polaron percolation’, and transport models that invoke magnons and phonons [35]. However, none have explained the peculiar transport and spatial behaviour for reasonable parameter values.

The problem remains difficult because (i) self trapping occurs in a finite temperature spatially correlated spin back-

ground, and (ii) the phenomena occurs at strong electron-spin coupling where we have no analytical tools for the electronic states. This forces one to use numerical approaches and there the difficulty is with accessible spatial scales. A single polaron, at realistic electron-spin coupling, can have a linear size  $\sim 10$  lattice spacings and a finite electron number  $N_{el}$ , to mimic finite density, in a two dimensional (2D) system will require  $\sim N_{el} \times 10^2$  lattice sites. This has remained out of reach, so neither FP formation nor its impact on magneto-transport and tunneling spectra have been addressed. We offer a computational advance that allows access to these features.

In the standard model of FPs [29–31] one has a ferromagnetic Heisenberg model, with coupling  $J$ , with the spins Kondo coupled to tight binding electrons (which have a hopping  $t$ ) through an interaction  $J'$ . The magnetic states of this model can be accessed by a Monte Carlo (MC) scheme that iteratively diagonalises the electron problem [29, 30, 36, 37]. For a lattice with  $N$  sites each microscopic update costs  $\mathcal{O}(N^3)$ , and a ‘system sweep’ costs  $\mathcal{O}(N^4)$ . This has limited studies to sizes  $\sim 10 \times 10$  [36, 37]. We set up a Langevin equation (LE) to evolve the spins in the presence of a thermal noise and sample configurations once equilibrium is reached. The diagonalisation cost for torque calculation is still  $\mathcal{O}(N^3)$  but now the spins can be updated in parallel, so the system update cost is also  $\mathcal{O}(N^3)$ . This advantage allow a breakthrough, with access to lattices upto  $20 \times 20$  and  $N_{el} \sim 10$  (density  $\sim 0.02$ ).

We use the LE approach on a 2D square lattice for parameters that are generally accepted for  $\text{EuB}_6$  to attempt as quantitative a match as possible. We set  $t = 100\text{meV}$ ,  $J'S = t$ ,  $JS^2 = 0.01t$ , [33, 34] and electron density  $n \sim 0.02$ , probing the system as a function of temperature  $T$  and magnetic field  $h$ . Our main results are the following:

1. *Spatial textures in tunneling*: Spatial textures in electron density and magnetisation, on the scale of  $6 - 8$  lattice spacings, exist over a window  $T \sim 0.7T_c - 1.5T_c$  at  $h = 0$ . The local density of states (LDOS) in the ‘polaronic’ regions have a distinct signature, with a peak at  $\sim 25$  meV below Fermi level. This ‘binding energy’ and the spatial scale are in excel-

lent agreement with experiment.

2. *Resistivity, magnetotransport:* The resistivity  $\rho(T)$  is nonmonotonic, with a peak near  $T_c$  and a shallow minimum at  $T \sim 1.5T_c$ . An applied field diminishes the peak-dip feature and suppresses it altogether by  $h \sim 1.0$  Tesla, consistent with  $\text{EuB}_6$  data.

3. *Optical conductivity:* We predict that the low frequency optical conductivity  $\sigma(\omega, T)$  should have the expected Drude character for  $T \ll T_c$  but by  $0.7T_c$  it would pick up a distinct non Drude form, with the peak in  $\sigma(\omega)$  shifting from  $\omega = 0$  to  $\omega \sim 0.1t$  by  $T_c$  and to  $\omega \sim 0.2t$  by  $2T_c$ .

4. *Physical mechanism:* The anomalies in local density of states and transport arise from (i) the separation of the occupied (below chemical potential,  $\mu$ ) states from the main body of the band by a weak pseudogap near  $T_c$ , and (ii) a non monotonic degree of localisation of states in the window  $\mu \pm k_B T$  as a function of temperature.

The Heisenberg-Kondo (H-K) model we study in 2D is:

$$H = -t \sum_{\langle ij \rangle, \sigma} c_{i\sigma}^\dagger c_{j\sigma} - J' \sum_i \mathbf{S}_i \cdot \vec{\sigma}_i - J \sum_{\langle ij \rangle} \mathbf{S}_i \cdot \mathbf{S}_j \quad (1)$$

The moments on Eu are large, with  $2S \gg 1$  so we treat them as classical unit vectors, absorbing the magnitude  $S$  in the coupling constants:  $J \rightarrow JS^2$  and  $J' \rightarrow J'S$ . The parameter values have been stated earlier, our electron number  $N_{el} = 10$ .

To generate equilibrium spin configurations  $\{\mathbf{S}_i\}$  we use a LE where the spins experience a torque (below) derived from  $H$  alongside a stochastic kick, with variance  $\propto k_B T$ , to model the effect of temperature. This method not only facilitates the exploration of equilibrium spin configurations but also enables the study of spin dynamics. The LE has the form:

$$\begin{aligned} \frac{d\mathbf{S}_i}{dt} &= \mathbf{S}_i \times (\mathbf{T}_i + \mathbf{h}_i) - \gamma \mathbf{S}_i \times (\mathbf{S}_i \times \mathbf{T}_i) \\ \mathbf{T}_i &= -\frac{\partial H}{\partial \mathbf{S}_i} = -J' \langle \vec{\sigma}_i \rangle - J \sum_{\delta} \mathbf{S}_j \delta_{j,i+\delta} \\ \langle h_{i\alpha} \rangle &= 0, \quad \langle h_{i\alpha}(t) h_{j\beta}(t') \rangle = 2\gamma k_B T \delta_{ij} \delta_{\alpha\beta} \delta(t-t') \end{aligned} \quad (2)$$

$\mathbf{T}_i$  is the effective torque acting on the spin at the  $i$ -th site,  $\gamma = 0.1$  is a damping constant, and  $\mathbf{h}_i$  is the thermal noise satisfying the fluctuation-dissipation theorem.  $\langle \vec{\sigma}_i \rangle$  represents the expectation of  $\vec{\sigma}_i$  taken over the instantaneous ground state of the electrons, and  $\delta$  is the set of nearest neighbours. In the presence of an external magnetic field there is an additional term  $\hat{z}h$  in  $\mathbf{T}_i$ . Once Langevin evolution reaches equilibrium the magnetic correlations can be computed from the  $\{\mathbf{S}_i\}$ , and electronic features obtained by diagonalisation in these backgrounds (see Supplement).

*Spatial textures in tunneling:* Fig.1 reproduces spatial textures observed experimentally [18] and compares them to our results. The top row shows the experimental maps of local conductance  $g(\mathbf{r}, V) = dI(\mathbf{r}, V)/dV$  in  $\text{EuB}_6$  at  $V = -24\text{mV}$ . We will call the measured conductance at  $V = -24\text{mV}$  as  $g_{ref}(\mathbf{r})$ . The map on the left reveals homogeneous behaviour of  $g_{ref}$  at  $T = 5.6\text{K}$  ( $\sim 0.4T_c$ ), which changes to a distinctly inhomogeneous behaviour at  $T = 20\text{K}$  ( $\sim 1.3T_c$ )

in the right plot. The linear dimension of the bright patches is  $\sim 8$  lattice spacings. The panels below the spatial maps show  $g(\mathbf{r}, V)$  averaged over the marked regions in the upper panel. In the low  $T$  case the  $g(V)$  trace does not depend on spatial location, while at  $1.3T_c$  it shows very different  $V < 0$  behaviour between the high  $g_{ref}$  and low  $g_{ref}$  areas, with a

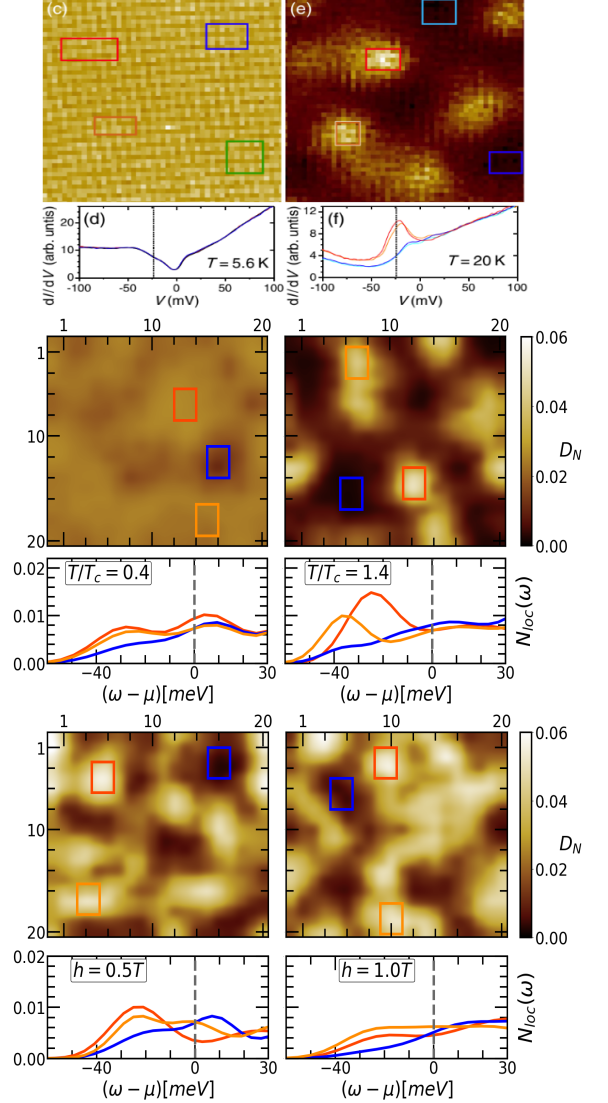


FIG. 1. Spatial map of tunneling conductance. Top row: Experimental map of local conductance  $g(\mathbf{r}, V) = dI(\mathbf{r}, V)/dV$  at  $V = -24\text{mV}$  at  $5.6\text{K}$  and  $20\text{K}$ , with  $T_c \sim 15\text{K}$ . At  $T = 5.6\text{K}$  the  $-24\text{mV}$  conductance is uniform. For  $T = 20\text{K}$  it is inhomogeneous - the bright patches are supposed to be the polaronic regions. The LDOS below shows that  $g(V)$  is site independent for  $T \ll T_c$  and strongly inhomogeneous for  $T > T_c$ . Middle row: Our  $h = 0$  results on density  $n(\mathbf{r})$  at  $T = 0.4T_c$  (left) - showing a homogeneous density, and  $T = 1.4T_c$  (right) - showing strong inhomogeneity. Corresponding LDOS panels show almost site independent LDOS at  $0.4T_c$  and a strongly site differentiated LDOS at  $1.4T_c$ . High  $n(\mathbf{r})$  regions have a peak at  $\sim -25\text{meV}$ . Bottom row:  $h$  dependence at  $T = 1.4T_c$ . Left -  $h = 0.5$  Tesla, right -  $1.0$  Tesla. Trend: progressive homogenisation of  $n(\mathbf{r})$  and a site independent LDOS.

prominent peak at  $V \sim -25\text{mV}$  in the high  $g_{ref}$  areas.

We directly calculate  $n(\mathbf{r})$ , the electron density, using an instantaneous equilibrium spin configuration at a temperature  $T$  as input and diagonalizing  $H$ . The spatial maps in the middle row show  $n(\mathbf{r})$  at  $T = 0.4T_c$  (left) and  $T = 1.4T_c$  (right). It is evident that at  $T = 0.4T_c$  carriers are distributed almost uniformly across the lattice. However, at  $T = 1.4T_c$  the density is strongly inhomogeneous. Since  $n(\mathbf{r}) = \int_{-\infty}^{\infty} d\omega N(\mathbf{r}, \omega) f(\omega)$ , where  $N(\mathbf{r}, \omega)$  is the LDOS and  $f(\omega)$  is the Fermi function, an inhomogeneity in  $n(\mathbf{r})$  implies a spatial variation of  $N(\mathbf{r}, \omega)$ .

Within the simplest approximation the tunneling conductance at bias  $V$  is proportional to the LDOS at  $\omega = eV$ , where  $e$  is the electron charge. We therefore plot our  $N(\mathbf{r}, \omega)$  as a proxy for  $g(\mathbf{r}, V)$ . As expected, at low  $T$  the  $N(\mathbf{r}, \omega)$  traces are almost site independent. In the textured regime the polaronic regions have a prominent peak at  $\omega \sim [-20, -30]\text{meV}$ . The corresponding experimental peaks are at  $\sim -25\text{mV}$ . The polaronic patches have size  $\sim 8 \times 4$  lattice spacings. The polaronic levels are centered roughly at  $\sim 25\text{meV}$  below the Fermi energy and the LDOS suggests a mild dip as we move into the unoccupied part of the band.

The bottom panels show the effect of an applied magnetic field  $h$  at  $T = T_c$ . At  $h = 0.5\text{ Tesla}$  (left) the white regions are already more spread out than at  $h = 0$  and the corresponding LDOS has less prominent peaks than at  $h = 0$ . At  $h = 1.0\text{ Tesla}$  (right) the polarons have ‘overlapped’ and essentially

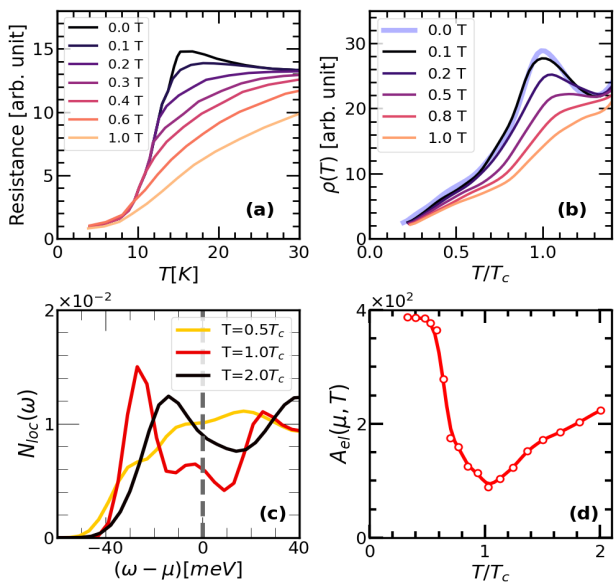


FIG. 2. Resistivity. (a) Temperature and field dependence of resistivity from experiments [17]. This is the total resistivity without any subtraction of a ‘phonon component’ etc. (b) Our result showing the prominent peak feature at  $h = 0$  and its complete suppression at  $h \sim 1\text{ Tesla}$ . (c) The LDOS in polaronic regions as a function of  $T$ , with a suppression near  $\mu$  when  $T \sim T_c$ . (d) The area associated with near chemical potential wavefunctions, averaged over  $\epsilon \sim \mu \pm k_B T$ , as a function of  $T$ . High degree of localisation near  $T_c$ .

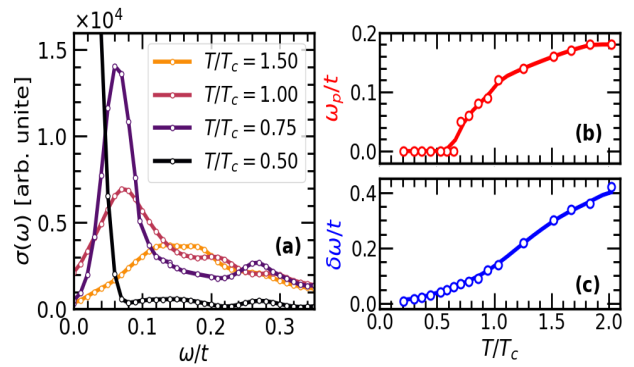


FIG. 3. (a) The low frequency behaviour of optical conductivity is demonstrated for various temperatures. The optical conductivity is plotted in measurable units along the y-axis and frequency is plotted along the x-axis scaled by hopping amplitude  $t$ . The temperature, in units of  $T_c$ , is represented through different colours in the plot. (b)  $T$  dependence of  $\omega_p$ , the peak location of  $\sigma(\omega)$ . Finite  $\omega_p$  indicates non Drude behaviour. (c)  $T$  dependence of  $\delta\omega$ , the full width at half maximum of  $\sigma(\omega)$ .

occupy the whole system. The density contrast is low, and the LDOS at the high density sites is only slightly different from that at the low density sites. We will see the impact in the transport properties next.

*Resistivity and magnetoresistance:* Unlike the monotonic  $T$  dependence in conventional ferromagnetic metals the resistivity  $\rho(T)$  in  $\text{EuB}_6$  has a peak at  $T \sim T_c$  a minimum near  $2T_c$ , and then rises again. The measured  $\rho(T, h)$  is shown in Fig.2(a) for  $T \leq 2T_c$ . The application of a magnetic field reduces the peak-dip feature, and by  $h \sim 0.3\text{ Tesla}$  it completely disappears. The experimental resistivity has a significant phonon contribution, with  $d\rho/dT > 0$ , which can be comparable to the magnetic scattering for  $T \gg T_c$  [19], so we compare our result, Fig.2(b), to the experiment only for  $T \lesssim 1.5T_c$ . Our  $h = 0$  resistivity has a ‘peak-dip’ feature, with a peak around  $T_c$  and a minimum at  $T \sim 1.4T_c$ , beyond which it rises again.  $\rho(T)$  in the window  $h = 0.1 - 1.0\text{ Tesla}$  shows a clear suppression of the  $d\rho/dT < 0$  behaviour with increasing  $h$ . By  $h = 1.0\text{ Tesla}$  the non-monotonicity is gone.

Non monotonic temperature dependence of resistivity, with a  $d\rho/dT < 0$  window, can arise either from the presence of a gap, or localisation of states near the chemical potential,  $\mu$ . Our global DOS does not show any gap in the relevant  $T$  window. However for  $T \sim 0.7T_c - 1.5T_c$  the polaronic regions show a LDOS,  $N_{loc}(\omega)$ , with enhancement for  $\omega < \mu$  and a weak suppression at  $\omega \sim \mu$ , Fig.2(c). This weak ‘pseudo-gap’ is absent both at  $T \ll T_c$  and  $T \gg T_c$ . In fact at larger coupling,  $J' = 5t$ , and for a single polaron, an actual ‘gap’ has been established before [30]. We also calculated  $A_{el}$ , the average spatial coverage of eigenstates in the energy window  $\epsilon \in (\mu \pm k_B T)$  (see Supplement). For  $T \ll T_c$  this is just system size,  $L^2$ , but for  $T \sim T_c$  this is only  $\mathcal{O}(9^2)$ , i.e. polaron size. It rises again as  $T$  grows beyond  $T_c$ , Fig.2(d). These observations do not constitute a ‘theory’ for  $\rho(T)$  near  $T_c$  but

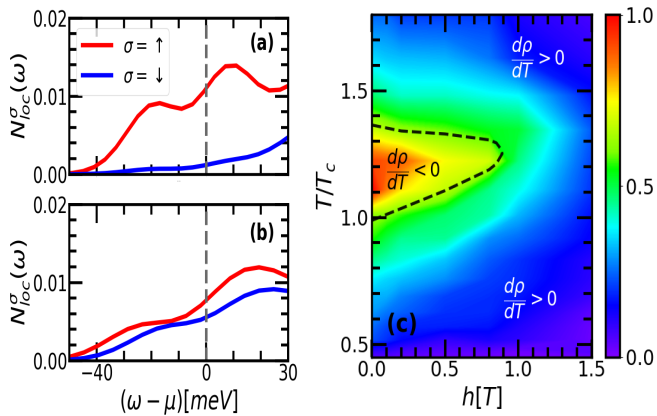


FIG. 4. Spin resolved LDOS and  $h - T$  phase diagram. (a) SRLDOS for  $h = 0.01T$  and  $T = T_c$  in the polaronic region, and (b) same for the non polaronic spatial regions. The red line represents the up spin component of the SRLDOS while the blue line represents the down spin component. (c) Map of the difference in integrated weight of up and down spin spectra taken over the spatially inhomogeneous regions, for varying  $h$  and  $T$ . The difference  $\delta W$  is maximum near  $T_c$  at  $h = 0$  and falls off either as  $T$  moves away or  $h$  is increased. There is no sharp boundary in terms of this quantity. The contour corresponding to  $d\rho/dT = 0$  (enclosing the  $d\rho/dT < 0$  regime) delineates prominent polaronic behaviour.

correlate non monotonicity in two simpler quantities with that observed in  $\rho(T)$ .

*Optical conductivity:* The temperature and field dependence of the resistivity correlate with the presence of electronic-magnetic textures in the system. We wanted to check whether the unusual electronic state had a signature in the optical conductivity  $\sigma(\omega)$  in the polaronic window. Most of the available data focus on high energies [11–13], where we think the effect of a low energy bound state like the polaron would be limited. Fig.3(a) shows our result over a window  $\omega = 0 - 0.3t$ , which would translate to  $\sim 0 - 30\text{meV}$  for  $\text{EuB}_6$ . We show this for four temperatures between  $0.5T_c$  and  $1.5T_c$ . At  $T = 0.5T_c$  where the magnetic state is highly polarised and the electronic state is essentially homogeneous we see a Drude response with a sharp peak at  $\omega = 0$  of width  $\sim 0.02t$ . The Drude feature sharpens as  $T \rightarrow 0$ . However as  $T$  increases we see that already by  $0.7T_c$  the peak location  $\omega_p$  has shifted to a finite value and the ‘d.c conductivity’ is strongly suppressed. This non Drude response persists to high  $T$ . In Fig.3(b) we show  $\omega_p(T)$  and in Fig.3(c) we show the width  $\delta\omega(T)$ .

*$h - T$  phase diagram:* We want to combine the results obtained on the various measurables to create a ‘polaronic phase diagram’ for  $\text{EuB}_6$ . While scanning tunneling (or LDOS) measurement is the most direct indicator of density inhomogeneity, by itself it does not reveal whether there is a large ‘polarisation’ in the high density region. A minor variation, probing the spin resolved LDOS (SRLDOS) in a small field, would not only indicate regions of high total density (by summing the up and down components) but also the extent of po-

larisation (from the difference of up and down components). Fig.4(a) shows the site-averaged SRLDOS for polaronic sites while Fig.4(b) shows it for the non polaronic sites, both at  $h = 0.01T$  and  $T = T_c$ . The up-down difference in 4(a), versus the up-down similarity in 4(b), is readily visible.

We compute  $\delta W = |W_{\uparrow} - W_{\downarrow}|$ , where  $W_{\uparrow} = -(1/\pi) \frac{1}{N_p} \sum_i \int_{-\infty}^{\mu} \text{Im}[N_{loc\ ii}^{\uparrow}(\omega)] d\omega$ , etc, where  $N_p$  is the number of sites in the polaronic region, and the sum runs over these  $N_p$  sites. We plot a normalised  $\delta W$  (dividing by its maximum value for any  $h, T$ ) with respect to  $h$  and  $T$  in Fig.4(c). There is no phase transition between the polaronic and non polaronic regimes, it is a crossover. There is a specific line one can draw, bounding the  $d\rho/dT < 0$  window and that is shown by the dashed line.

Finally, We discuss a few issues which have bearing on the theory-experiment comparison. (i) Effect of changing  $J'$ : we have checked that polarons are not stable below  $J' \sim 0.5t$ . For  $0.5t < J < 2t$  there is a peak-dip feature in  $\rho(T)$ . The peak-dip height difference increases with  $J'$  but the associated temperature window remains roughly  $J'$  independent. (ii) Effect of impurities: we have not done a full calculation including impurities but anticipate that low enough disorder (in 3D) will leave the low  $T$  behaviour intact but can enhance the  $d\rho/dT < 0$  window in temperature. It will also introduce pinning centers for the polarons. (iii) Effect of dimensionality: the physical process that leads to FP formation is dimension independent but some of the pathologies related to 2D, e.g, disorder induced localisation, or lack of long range order at finite  $T$ , will be absent. We will present some results separately. (iv) Several materials consisting of rare earth elements, such as  $\text{EuS}$ ,  $\text{EuO}$ , and  $\text{GdN}$ , exhibit ferromagnetic ground states and low magnetic transition temperatures (12K-70K), and show nonmonotonic resistivity. Typically, the resistivity peak occurs around  $T_c$ , but the peak-to-dip ratios differ. Although the variation in the peak-to-dip ratio can be captured by varying  $J'/t$  and carrier density the strongly insulating high  $T$  behaviour in some materials, we think, requires the inclusion of pinning centers.

*Conclusions:* We resolve the longstanding problem of transport and spectral features in  $\text{EuB}_6$ , the candidate material for ferromagnetic polarons, by using an exact diagonalisation based Langevin approach for the thermal state of low density electrons coupled to a Heisenberg spin system. We use intermediate electron-spin coupling, as suggested by experiments, and find a non monotonic resistivity with a small peak near  $T_c$ . Our spatially resolved tunneling density of states shows a striking inhomogeneity in a temperature window near  $T_c$ , with spatial scale and spectral features that are in excellent agreement with recent experiments. The resistivity and tunneling features are related to a strongly temperature dependent pseudogap in the electronic spectrum and the localisation of near Fermi level states. We make two specific predictions: (i) the optical conductivity would evolve from a Drude response at  $T \ll T_c$  to having a finite frequency peak, with characteristic location and width, as  $T \rightarrow T_c$ , and (ii) polaronic signatures,

indicated by the spin resolved local density of states, would be limited in  $\text{EuB}_6$  to  $T \sim 0.7T_c - 1.5T_c$  and  $h \sim 0 - 1$  Tesla. Our approach, augmented by the presence of pinning centers, can address supposed polaronic signatures in a host of rare earth materials.

We acknowledge use of the HPC facility at HRI.

- 
- [1] R. R. Heikes and C. W. Chen, Evidence for impurity bands in La-doped EuS, *Physics Physique Fizika* **1**, 159 (1964).
- [2] S. von Molnar and S. Methfessel, *J. Appl. Phys.* **38**, 959 (1967).
- [3] Z. Yang, X. Bao, S. Tan, and Y. Zhang, Magnetic polaron conduction in the colossal magnetoresistance material  $\text{Fe}_{1-x}\text{Cd}_x\text{Cr}_2\text{S}_4$ , *Phys. Rev. B* **69**, 144407 (2004).
- [4] Li, H., Xiao, Y., Schmitz, B. et al. Possible magnetic-polaron-switched positive and negative magnetoresistance in the GdSi single crystals. *Sci Rep* **2**, 750 (2012).
- [5] F. Natali, B. J. Ruck, H. J. Trodahl, Do Le Binh, S. Veizan, B. Damlano, Y. Cordier, F. Semond, and C. Meyer, Role of magnetic polarons in ferromagnetic GdN, *Phys. Rev. B* **87**, 035202 (2013).
- [6] Molnar, S. von, Static and Dynamic Properties of the Insulator–Metal Transition in Magnetic Semiconductors, Including the Perovskites. *Journal of Superconductivity* **14**, 199–204 (2001).
- [7] M Ziese, Extrinsic magnetotransport phenomena in ferromagnetic oxides, *Rep. Prog. Phys.* **65** 143 (2002).
- [8] C. Lin, C. Yi, Y. Shi, L. Zhang, G. Zhang, Jens Müller, and Y. Li, Spin correlations and colossal magnetoresistance in  $\text{HgCr}_2\text{Se}_4$ , *Phys. Rev. B* **94**, 224404 (2016).
- [9] S. Kimura, T. Nanba, S. Kunii, and T. Kasuya, Interband Optical Spectra of Rare-Earth Hexaborides, *J. Phys. Soc. Jpn.* **59**, pp. 3388–3392 (1990).
- [10] S. Kimura, T. Ito, H. Miyazaki, T. Mizuno, T. Iizuka, and T. Takahashi, Electronic inhomogeneity EuO: Possibility of magnetic polaron states, *Phys. Rev. B* **78**, 052409 (2008).
- [11] S. Kimura, T. Nanba, S. Kunii, and T. Kasuya, Interband Optical Spectra of Rare-Earth Hexaborides, *J. Phys. Soc. Jpn.* **59**, pp. 3388–3392 (1990).
- [12] L. Degiorgi, E. Felder, H. R. Ott, J. L. Sarrao, and Z. Fisk, Low-Temperature Anomalies and Ferromagnetism of  $\text{EuB}_6$ , *Phys. Rev. Lett.* **79**, 5134 (1997).
- [13] J. Kim, Y.-J. Kim, J. Kuneš, B. K. Cho, and E. J. Choi, "Optical spectroscopy and electronic band structure of ferromagnetic  $\text{EuB}_6$ ," *Phys. Rev. B*, **78**, 165120 (2008).
- [14] P. Nyhus, S. Yoon, M. Kauffman, S. L. Cooper, Z. Fisk, and J. Sarrao, Spectroscopic study of bound magnetic polaron formation and the metal-semiconductor transition in  $\text{EuB}_6$ , *Phys. Rev. B* **56**, 2717 (1997).
- [15] M. L. Brooks, T. Lancaster, S. J. Blundell, W. Hayes, F. L. Pratt, and Z. Fisk, Magnetic phase separation in  $\text{EuB}_6$  detected by muon spin rotation, *Phys. Rev. B* **70**, 020401(R) (2004).
- [16] S. Massidda, A. Continenza, T.M. de Pascale, and R. Monnier, Electronic structure of divalent hexaborides, *Physica B- Condensed Matter* **102**, 83–89(1996).
- [17] X. Zhang, L. Yu, S. von Molnár, Z. Fisk, and P. Xiong, Non-linear Hall Effect as a Signature of Electronic Phase Separation in the Semimetallic Ferromagnet  $\text{EuB}_6$ , *Phys. Rev. Lett.* **103**, 106602 (2009).
- [18] M. Pohlit, S. Rößler, Y. Ohno, H. Ohno, S. von Molnár, Z. Fisk, J. Müller, and S. Wirth, Evidence for Ferromagnetic Clusters in the Colossal-Magnetoresistance Material  $\text{EuB}_6$ , *Phys. Rev. Lett.* **120**, 257201 (2018).
- [19] S. Süllo, I. Prasad, M. C. Aronson, S. Bogdanovich, J. L. Sarrao, and Z. Fisk, Metallization and magnetic order in  $\text{EuB}_6$ , *Phys. Rev. B* **62**, 11626 (2000).
- [20] S. Paschen, D. Pushin, M. Schlatter, P. Vonlanthen, H. R. Ott, D. P. Young, and Z. Fisk, Electronic transport in  $\text{Eu}_{1-x}\text{Ca}_x\text{B}_6$ , *Phys. Rev. B* **61**, 4174 (2000).
- [21] G. Caimi, A. Perucchi, L. Degiorgi, H. R. Ott, V. M. Pereira, A. H. Castro Neto, A. D. Bianchi, and Z. Fisk, Magneto-Optical Evidence of Double Exchange in a Percolating Lattice, *Phys. Rev. Lett.* **96**, 016403 (2006).
- [22] P. Das, A. Aryan, J. Brandenburg, J. Müller, P. Xiong, S. von Molnár, and Z. Fisk, Magnetically driven electronic phase separation in the semimetallic ferromagnet  $\text{EuB}_6$ , *Phys. Rev. B* **86**, 184425 (2012).
- [23] J. Kim, W. Ku, C.-C. Lee, D. S. Ellis, B. K. Cho, A. H. Said, Y. Shvyd'ko, and Y.-J. Kim, Spin-split conduction band in  $\text{EuB}_6$  and tuning of half-metallicity with external stimuli, *Phys. Rev. B* **87**, 155104 (2013).
- [24] R. S. Manna, P. Das, M. de Souza, F. Schnelle, M. Lang, J. Müller, S. von Molnár, and Z. Fisk, Lattice Strain Accompanying the Colossal Magnetoresistance Effect in  $\text{EuB}_6$ , *Phys. Rev. Lett.* **113**, 067202 (2014).
- [25] S. Rößler, L. Jiao, S. Seiro, P. F. S. Rosa, Z. Fisk, U. K. Rößler, and S. Wirth, Visualization of localized perturbations on a (001) surface of the ferromagnetic semimetal  $\text{EuB}_6$ , *Phys. Rev. B* **101**, 235421 (2020).
- [26] C. Min, B. Kang, B. K. Cho, E.-J. Cho, B.-G. Park, and H.-D. Kim, Semimetallic nature of and magnetic polarons in  $\text{EuB}_6$  studied using angle-resolved photoemission spectroscopy, *J. Korean Phys. Soc.* **79**, 734740 (2021).
- [27] S.-Y. Gao, S. Xu, H. Li, C.-J. Yi, S.-M. Nie, Z.-C. Rao, H. Wang, Q.-X. Hu, X.-Z. Chen, W.-H. Fan, J.-R. Huang, Y.-B. Huang, N. Pryds, M. Shi, Z.-J. Wang, Y.-G. Shi, T.-L. Xia, T. Qian, and H. Ding, Time-Reversal Symmetry Breaking Driven Topological Phase Transition in  $\text{EuB}_6$ , *Phys. Rev. X* **11**, 021016 (2021).
- [28] G. Beaudin, L. M. Fournier, A. D. Bianchi, M. Nicklas, M. Kenzelmann, M. Laver, and W. Witczak-Krempa, Possible quantum nematic phase in a colossal magnetoresistance material, *Phys. Rev. B* **105**, 035104 (2022).
- [29] P. Majumdar and P. Littlewood, Magnetoresistance in Mn Pyrochlore: Electrical Transport in a Low Carrier Density Ferromagnet, *Phys. Rev. Lett.* **81**, 1314 (1998).
- [30] M. J. Calderón, L. Brey, and P. B. Littlewood, Stability and dynamics of free magnetic polarons, *Phys. Rev. B* **62**, 3368 (2000).
- [31] Tao Liu, Mang Feng, Kelin Wang, A variational study of the self-trapped magnetic polaron formation in double-exchange model, *Physics Letters A*, Volume 337, Issues 4–6, 2005.
- [32] L. Craco, C. I. Ventura, A. N. Yaresko, and E. Müller-Hartmann, Mott-Hubbard quantum criticality in paramagnetic CMR pyrochlores, *Phys. Rev. B* **73**, 094432 (2006).
- [33] L. G. L. Wegener and P. B. Littlewood, Fluctuation-induced hopping and spin-polaron transport, *Phys. Rev. B* **66**, 224402 (2002).
- [34] M. J. Calderón, L. G. L. Wegener, and P. B. Littlewood, Evaluation of evidence for magnetic polarons in  $\text{EuB}_6$ , *Phys. Rev. B* **70**, 092408 (2004).
- [35] J. Chatterjee, U. Yu, and B. I. Min, Spin-polaron model: Transport properties of  $\text{EuB}_6$ , *Phys. Rev. B* **69**, 134423 (2004).
- [36] U. Yu and B. I. Min, Magnetic and Transport Properties of the Magnetic Polaron: Application to  $\text{Eu}_{1-x}\text{La}_x\text{B}_6$  System, *Phys.*

Rev. Lett. **94**, 117202 (2005).

[37] U. Yu and B. I. Min, Magnetic-phase transition in the magnetic-polaron system studied with the Monte Carlo method: Anomalous specific heat of EuB6, Phys. Rev. B **74**, 094413 (2006)

## Supplementary Material

### Computation of electronic properties

Let the equilibrium spin configurations generated by the Langevin equation at some temperature  $T$  be indexed by a label  $\alpha$ , i.e, the spin configurations are  $\{\mathbf{S}_i\}_\alpha$ . The corresponding set of single particle eigenvalues would be  $\epsilon_n^\alpha$  and the eigenstates would be  $\psi_n^\alpha(\mathbf{r})$ . The electron spin is not a quantum number in a generic  $\mathbf{S}_i$  configuration so the index  $n$  has  $2N$  values where  $N$  is the number of lattice sites. In what follows  $f(\epsilon) = (e^{\beta(\epsilon-\mu)} + 1)^{-1}$  is the Fermi function.

We first write the expressions for various electronic properties in a specific configuration  $\alpha$ . Since the system is translation invariant, i.e, without any extrinsic disorder, quantities like local density and LDOS will be site independent on configuration averaging. For them the results we show pertain to single configurations. For the optical conductivity and resistivity, however, configuration average is meaningful and we do so over typically 100 configurations.

#### 1. Spatial density:

$$n_\alpha(\mathbf{r}) = \sum_n |\psi_n^\alpha(\mathbf{r})|^2 f(\epsilon_n^\alpha) \quad (3)$$

#### 2. Density of states.

$$N_\alpha(\omega) = \sum_n \delta(\omega - \epsilon_n^\alpha) \quad (4)$$

#### 3. Local density of states.

$$N_\alpha(\mathbf{r}, \omega) = \sum_n |\psi_n^\alpha(\mathbf{r})|^2 \delta(\omega - \epsilon_n^\alpha) \quad (5)$$

#### 4. Spin resolved DOS: the LDOS above is spin summed. To know if there is a large local magnetisation over a spatial neighbourhood it is useful to calculate the

spin resolved LDOS from the local Greens function  $G_{\sigma\sigma}^\alpha(\mathbf{r}, \omega)$ .

$$N_\sigma^\alpha(\mathbf{r}, \omega) = -\left(\frac{1}{\pi}\right) \text{Im}[G_{\sigma\sigma}^\alpha(\mathbf{r}, \omega)]$$

$$G_{\sigma\sigma}^\alpha(\mathbf{r}, \omega) = \int_0^\infty dt e^{i\omega t} \langle \Psi_\alpha^0 | [c_{\mathbf{r}\sigma}(t), c_{\mathbf{r}\sigma}^\dagger(0)] | \Psi_\alpha^0 \rangle \quad (6)$$

where  $|\Psi_\alpha^0\rangle$  is the many body ground state of the  $N_{el}$  system (here we ignore Fermi factors).

#### 5. Optical conductivity.

$$\sigma_\alpha(\omega) = A \sum_{m,n} \frac{f(\epsilon_m^\alpha) - f(\epsilon_n^\alpha)}{\epsilon_m^\alpha - \epsilon_n^\alpha} |\hat{j}_{mn}^{\alpha\alpha}|^2 \delta(\omega - (\epsilon_m^\alpha - \epsilon_n^\alpha))$$

$$\hat{j} = ita_0 e \sum_{i,\sigma} (c_{i+xa_0,\sigma}^\dagger c_{i,\sigma} - h.c) \quad (7)$$

where  $A = \pi e^2 / \hbar N$

#### 6. DC resistivity: we obtained the ‘dc conductivity’ $\sigma_\alpha$ as

$$\sigma_\alpha = \frac{1}{\Delta\omega} \int_0^{\Delta\omega} d\omega \sigma_\alpha(\omega) \quad (8)$$

where  $\Delta\omega$  is a small multiple of the average finite size gap in the spectrum. In our calculations it is  $0.05t$ . The d.c resistivity is the inverse of the thermally averaged conductivity

$$\rho = \frac{1}{N_\alpha} \sum_\alpha \frac{1}{\sigma_\alpha}$$

#### 7. Inverse participation ratio (IPR): this is useful to quantify the inverse of the ‘volume’ associated with a single particle eigenstates. The standard definition, for normalised states, is:

$$I_n^\alpha = \int d\mathbf{r} |\psi_n^\alpha(\mathbf{r})|^4 \quad (9)$$

D.c transport involves states over a window  $\mu \pm k_B T$ . Since the character of states changes rapidly with energy in the polaronic regime we calculate the typical area  $A(T)$  associated with eigenstates in the  $\mu \pm k_B T$  window as follows:

$$A_\alpha(T) = \frac{1}{N_S} \sum_n \frac{1}{I_n^\alpha}, \quad \epsilon_n \in (\mu \pm k_B T) \quad (10)$$

where  $N_S$  is the number of states in the  $\mu \pm k_B T$  window. We then average  $A_\alpha$  over configurations.